Solar Modulation of Cosmic Nuclei over a Solar Cycle: Results from the Alpha Magnetic Spectrometer

M. Aguilar,[29] B. Alpat,[35] G. Ambrosi,[35] H. Anderson,[10] L. Arruda,[27] N. Attig,[24] C. Bagwell,[10] F. Barao,[27] M. Barbanera,[35] L. Barrin,[14] A. Bartoloni,[39] R. Battiston,[46,47] A. Bayyari,[20] N. Belyaev,[10] B. Bertucci,[35,36] V. Bindi,[20] K. Bollweg,[21] J. Bolster,[10] M. Borchiellini,[17] B. Borgia,[39,40] M. J. Boschini,[31] M. Bourquin,[15] C. Brugnoni,[35,36] J. Burger,[10] W. J. Burger,[46] N. Burzillà,[41] X. D. Cai,[10] M. Capell,[10] J. Casaus,[29] G. Castellini,[13] F. Cervelli,[37] Y. H. Chang,[44] G. M. Chen,[6,7] G. R. Chen,[23] H. Chen,[19] H. S. Chen,[6,7] Y. Chen,[23] L. Cheng,[23] H. Y. Chou,[44] S. Chouridou,[1] V. Choutko,[10] C. H. Chung,[1] C. Clark,[10,21] G. Coignet,[3] C. Consolandi,[20] A. Contin,[8,9] C. Corti,[20] Z. Cui,[22,23] K. Dadzie,[10] F. D'Angelo,[9,8] A. Dass,[46,47] C. Delgado,[29] S. Della Torre,[31] M. B. Demirköz,[2] L. Derome,[16] S. Di Falco,[37] V. Di Felice,[41] C. Díaz,[29] F. Dimiccoli,[46,47] P. von Doetinchem,[20] F. Dong,[33] M. Duranti,[35] A. Egorov,[10] A. Eline,[10] F. Faldi,[35,36] D. Fehr,[1] J. Feng,[18] E. Fiandrini,[35,36] P. Fisher,[10] V. Formato,[41] R. J. García-López,[26] C. Gargiulo,[14] H. Gast,[1] M. Gervasi,[31,32] F. Giovacchini,[29] D. M. Gómez-Coral,[30] J. Gong,[33] D. Grandi,[31,32] M. Graziani,[35,36] S. Haino,[44] K. C. Han,[28] R. K. Hashmani,[2] Z. H. He,[18] B. Heber,[25] F. Hernández-Nicolás,[29] T. H. Hsieh,[10] J. Y. Hu,[35] B. W. Huang,[19] M. Ionica,[35] M. Incagli,[37] Yi Jia,[10] H. Jinchi,[28] G. Karagöz,[2] Th. Kirn,[1] A. P. Klipfel,[10] O. Kounina,[10] A. Kounine,[10] V. Koutsenko,[10] D. Krasnopevtsev,[10] A. Kuhlman,[20] A. Kulemzin,[10] G. La Vacca,[31,32] E. Laudi,[14] G. Laurenti,[8] G. LaVecchia,[10] I. Lazzizzera,[46,47] H. T. Lee,[43] S. C. Lee,[44] H. L. Li,[23] J. H. Li,[22] J. Q. Li,[33] M. Li,[15] M. Li,[22] Q. Li,[33] Q. Li,[22] Q. Y. Li,[23] S. Li,[1] S. L. Li,[6] Z. H. Li,[6,7] M. J. Liang,[6,7] P. Liao,[22] C. H. Lin,[44] T. Lippert,[24] J. H. Liu,[5] P. C. Liu,[23] Z. Liu,[41] S. Q. Lu,[6,44] Y. S. Lu,[6,†] J. Z. Luo,[33] Q. Luo,[18] S. D. Luo,[19] Xi Luo,[23] C. Mañá,[29] J. Marín,[29] J. Marquardt,[25] G. Martínez,[29] N. Masi,[8] D. Maurin,[16] T. Medvedeva,[10] A. Menchaca-Rocha,[30] Q. Meng,[33] V. V. Mikhailov,[23] M. Molero,[26] P. Mott,[10,21] L. Mussolin,[35,36] Y. Najafi Jozani,[1] R. Nicolaidis,[47,46] N. Nikonov,[20] F. Nozzoli,[46] J. Ocampo-Peleteiro,[29] A. Oliva,[8] M. Orcinha,[35,36] F. Palmonari,[8,9] M. Paniccia,[15] A. Pashnin,[10] M. Pauluzzi,[35,36] D. Pelosi,[35,36] S. Pensotti,[31,32] P. Pietzcker,[25] V. Plyaskin,[10] S. Poluianov,[34] D. Pridöhl,[1] Z. Y. Qu,[23] L. Quadrani,[8,9] P. G. Rancoita,[31] D. Rapin,[15] A. Reina Conde,[8] E. Robyn,[8] I. Rodríguez-García,[29] L. Romaneehsen,[25] F. Rossi,[47,46] A. Rozhkov,[10] D. Rozza,[31,32] R. Sagdeev,[11] S. Schael,[1] A. Schultz von Dratzig,[1] G. Schwering,[1] E. S. Seo,[12] B. S. Shan,[4] A. Shukla,[20] T. Siedenburg,[1] A. Siemko,[10] G. Silvestre,[35] J. W. Song,[22] X. J. Song,[23] R. Sonnabend,[1] L. Strigari,[39,*] T. Su,[23] Q. Sun,[22] Z. T. Sun,[6] L. Tabarroni,[41] M. Tacconi,[31,32] Z. C. Tang,[6] J. Tian,[41] Y. Tian,[19] Samuel C. C. Ting,[10,14] S. M. Ting,[10] N. Tomassetti,[35,36] J. Torsti,[48] A. Ubaldi,[35,36] T. Urban,[10,21] I. Usoskin,[34] V. Vagelli,[38,35] R. Vainio,[48] P. Väisänen,[35,36] M. Valencia-Otero,[45] E. Valente,[39,40] E. Valtonen,[48] M. Vázquez Acosta,[26] M. Vecchi,[17] M. Velasco,[29] C. X. Wang,[22] J. C. Wang,[6] L. Wang,[5] L. Q. Wang,[22] N. H. Wang,[22] Q. L. Wang,[5] S. Wang,[20] X. Wang,[10] Z. M. Wang,[23] J. Wei,[15,23] Z. L. Weng,[10] H. Wu,[33] Y. Wu,[23] Z. B. Wu,[22] J. N. Xiao,[19] R. Q. Xiong,[33] X. Z. Xiong,[19] W. Xu,[22,23] Q. Yan,[10] H. T. Yang,[6,7] Y. Yang,[42] H. Yi,[33] Y. H. You,[6,7] Y. M. Yu,[10] Z. Q. Yu,[6] C. Zhang,[6] F. Z. Zhang,[6] J. Zhang,[22] J. H. Zhang,[33] Z. Zhang,[10] P. W. Zhao,[18] C. Zheng,[23] Z. M. Zheng,[4] H. L. Zhuang,[6] V. Zhukov,[1] A. Zichichi,[8,9] M. Zuberi,[10] and P. Zuccon[46,47]

(AMS Collaboration)

[1]*I. Physics Institute and JARA-FAME, RWTH Aachen University, 52056 Aachen, Germany*
[2]*Department of Physics, Middle East Technical University (METU), 06800 Ankara, Türkiye*
[3]*Université Grenoble Alpes, Université Savoie Mont Blanc, CNRS, LAPP-IN2P3, 74000 Annecy, France*
[4]*Beihang University (BUAA), Beijing 100191, China*
[5]*Institute of Electrical Engineering (IEE), Chinese Academy of Sciences, Beijing 100190, China*
[6]*Institute of High Energy Physics (IHEP), Chinese Academy of Sciences, Beijing 100049, China*
[7]*University of Chinese Academy of Sciences (UCAS), Beijing 100049, China*
[8]*INFN Sezione di Bologna, 40126 Bologna, Italy*
[9]*Università di Bologna, 40126 Bologna, Italy*
[10]*Massachusetts Institute of Technology (MIT), Cambridge, Massachusetts 02139, USA*
[11]*East-West Center for Space Science, University of Maryland, College Park, Maryland 20742, USA*
[12]*IPST, University of Maryland, College Park, Maryland 20742, USA*
[13]*CNR–IROE, 50125 Firenze, Italy*
[14]*European Organization for Nuclear Research (CERN), 1211 Geneva 23, Switzerland*
[15]*DPNC, Université de Genève, 1211 Genève 4, Switzerland*
[16]*Université Grenoble Alpes, CNRS, Grenoble INP, LPSC-IN2P3, 38000 Grenoble, France*

[17]Kapteyn Astronomical Institute, University of Groningen, P.O. Box 800, 9700 AV Groningen, Netherlands
[18]Sun Yat–Sen University (SYSU), Guangzhou 510275, China
[19]Zhejiang University (ZJU), Hangzhou 310058, China
[20]Physics and Astronomy Department, University of Hawaii, Honolulu, Hawaii 96822, USA
[21]National Aeronautics and Space Administration Johnson Space Center (JSC), Houston, Texas 77058, USA
[22]Shandong University (SDU), Jinan, Shandong 250100, China
[23]Shandong Institute of Advanced Technology (SDIAT), Jinan, Shandong 250100, China
[24]Jülich Supercomputing Centre and JARA-FAME, Research Centre Jülich, 52425 Jülich, Germany
[25]Institut für Experimentelle und Angewandte Physik, Christian-Albrechts-Universität zu Kiel, 24118 Kiel, Germany
[26]Instituto de Astrofísica de Canarias (IAC), 38205 La Laguna, and Departamento de Astrofísica, Universidad de La Laguna, 38206 La Laguna, Tenerife, Spain
[27]Laboratório de Instrumentação e Física Experimental de Partículas (LIP), 1649-003 Lisboa, Portugal
[28]National Chung–Shan Institute of Science and Technology (NCSIST), Longtan, Tao Yuan 32546, Taiwan
[29]Centro de Investigaciones Energéticas, Medioambientales y Tecnológicas (CIEMAT), 28040 Madrid, Spain
[30]Instituto de Física, Universidad Nacional Autónoma de México (UNAM), Ciudad de México 01000, Mexico
[31]INFN Sezione di Milano–Bicocca, 20126 Milano, Italy
[32]Università di Milano–Bicocca, 20126 Milano, Italy
[33]Southeast University (SEU), Nanjing 210096, China
[34]Sodankylä Geophysical Observatory and Space Physics and Astronomy Research Unit, University of Oulu, 90014 Oulu, Finland
[35]INFN Sezione di Perugia, 06100 Perugia, Italy
[36]Università di Perugia, 06100 Perugia, Italy
[37]INFN Sezione di Pisa, 56100 Pisa, Italy
[38]Agenzia Spaziale Italiana (ASI), 00133 Roma, Italy
[39]INFN Sezione di Roma 1, 00185 Roma, Italy
[40]Università di Roma La Sapienza, 00185 Roma, Italy
[41]INFN Sezione di Roma Tor Vergata, 00133 Roma, Italy
[42]National Cheng Kung University, Tainan 70101, Taiwan
[43]Academia Sinica Grid Center (ASGC), Nankang, Taipei 11529, Taiwan
[44]Institute of Physics, Academia Sinica, Nankang, Taipei 11529, Taiwan
[45]Physics Department and Center for High Energy and High Field Physics, National Central University (NCU), Tao Yuan 32054, Taiwan
[46]INFN TIFPA, 38123 Trento, Italy
[47]Università di Trento, 38123 Trento, Italy
[48]Space Research Laboratory, Department of Physics and Astronomy, University of Turku, 20014 Turku, Finland

(Received 9 October 2024; accepted 22 November 2024; published 3 February 2025)

We report the properties of precision time structures of cosmic nuclei He, Li, Be, B, C, N, and O fluxes over an 11-year solar cycle from May 2011 to November 2022 in the rigidity range from 1.92 to 60.3 GV. The nuclei fluxes show similar but not identical time variations with amplitudes decreasing with increasing rigidity. In particular, below 3.64 GV the Li, Be, and B fluxes, and below 2.15 GV the C, N, and O fluxes, are significantly less affected by solar modulation than the He flux. We observe that these differences in solar modulation are linearly correlated with the differences in the spectral indices of the cosmic nuclei fluxes. This shows, in a model-independent way, that solar modulation of galactic cosmic nuclei depends on their spectral shape. In addition, solar modulation differences due to nuclei velocity dependence on the mass-to-charge ratio (A/Z) are not observed.

DOI: 10.1103/PhysRevLett.134.051001

Cosmic rays entering the heliosphere are subject to diffusion, convection, adiabatic energy losses, and magnetic drift, as described by the Parker equation [1]. The temporal evolution of these processes leads to cosmic-ray intensity variations that correlate with solar activity, which has several cycles [2]. The most significant is the 11-year solar cycle during which the number of sunspots changes from minimum to maximum and then back to a minimum. Cosmic-ray transport in the heliosphere is rigidity-dependent. Hence, the

*Also at IRCCS Azienda Ospedaliero-Universitaria di Bologna, Bologna, Italy.
†Deceased.

different nuclei fluxes are expected to have similar time variations at a given rigidity. However, according to the Parker equation, the time variation of fluxes of different cosmic-ray nuclei may differ due to (i) differences in the spectral shape of cosmic rays entering the heliosphere, and (ii) differences arising from the velocity dependence of the solar modulation for cosmic rays with a different mass-to-charge ratio (A/Z) [3–5].

Previously, AMS observed that nuclei with $2 \leq Z \leq 8$ in cosmic rays belong to three groups with distinctly different rigidity spectra [6–9]: the He, C, and O, which are mostly primary, that is, produced and accelerated in astrophysical sources; the secondaries Li, Be, and B, which are produced from the interaction of primaries with the interstellar medium; and N, which is a combination of primary and secondary components.

AMS previously measured the time variations of the electron, positron, proton, antiproton, and helium fluxes [10–14]. Significant differences in solar modulation have been observed among these particles. Furthermore, the study of the time variation of hydrogen and helium isotopes, p, D, ^{3}He, and ^{4}He, revealed a significantly different solar modulation behavior for different isotopes [15,16].

In this Letter we present the time evolution of cosmic-ray nuclei fluxes He, Li, Be, B, C, N, O in the rigidity range from 1.92 to 60.3 GV measured for 147 Bartels rotations from May 2011 to November 2022. The measurements are based on 9.61×10^8 He, 5.3×10^6 Li, 2.6×10^6 Be, 7.8×10^6 B, 26.1×10^6 C, 6.6×10^6 N, and 22.1×10^6 O nuclei.

Detector—The description of the AMS detector is presented in Ref. [17] and shown in Fig. S1 of the Supplemental Material (SM) [18]. The key elements used in this measurement are the permanent magnet [19], the silicon tracker [20], and the four planes of time of flight scintillation counters [21]. AMS also contains a transition radiation detector, a ring imaging Čerenkov detector, an electromagnetic calorimeter, and an array of anticoincidence counters. Details on the detector, trigger, and Monte Carlo (MC) simulation are contained in Refs. [6,22–25] and in the SM [18].

Event selection—AMS collected 2.12×10^{11} cosmic-ray events from May 2011 to November 2022. Nuclei events are required to be downward going, to have a reconstructed track in the inner tracker, and to pass through the first tracker layer $L1$. See Fig. S2 of SM [18] for a reconstructed O event. Details of the event selection and background subtraction are contained in Refs. [7–9,26] and in the SM [18].

Data analysis—For a given Bartels rotation, the isotropic flux Φ_X^i for a nucleus X in the ith rigidity bin $(R_i; R_i + \Delta R_i)$ is given by

$$\Phi_X^i = \frac{N_X^i}{A_X^i \epsilon_X^i T_i \Delta R_i}, \tag{1}$$

where N_X^i is the number of events corrected for bin-to-bin migration, A_X^i is the effective acceptance, ϵ_X^i is the trigger efficiency, and T_i is the collection time. In this Letter, fluxes were measured in 40 rigidity bins from 1.92 to 60.3 GV. Bin-to-bin rigidity migration of events due to the finite rigidity resolution was corrected using the unfolding procedures described in Ref. [6] independently for each Bartels rotation.

Extensive studies were made of the systematic errors. These errors include the uncertainties in the background evaluation, the trigger efficiency, the acceptance calculation, the absolute rigidity scale, the rigidity resolution function, and the unfolding procedure.

The overall uncertainty due to background subtraction is negligible ($< 0.5\%$) for He, C, and O, and is $< 0.8\%$ for Li, $< 1.2\%$ for Be, $< 1.2\%$ for B, and $< 1.1\%$ for N over the entire rigidity range.

The systematic error on the nuclei fluxes associated with the trigger efficiency measurement is negligible over the entire rigidity range.

The effective acceptances were calculated using MC simulation and corrected for small differences between the data and simulated events related to (a) event reconstruction and selection, namely in the efficiencies of velocity vector determination, track finding, charge determination, and tracker quality cuts, and (b) the details of inelastic interactions of nuclei in the AMS materials. The systematic error in each flux associated with the reconstruction and selection between MC simulation and data is $< 1\%$ over the entire rigidity range.

The material traversed by nuclei within AMS is composed primarily of carbon and aluminum. The survival probabilities of nuclei due to interactions in the materials were measured using cosmic-ray data collected by AMS as described in Ref. [27]. The systematic error due to uncertainties in the evaluation of the inelastic cross sections leads to a systematic error of $< 2\%$ for all the nuclei over the entire rigidity range.

A time-dependent systematic error due to the variations of reconstruction efficiencies for each Bartels rotation was estimated to be $< 1\%$ for He, $< 0.9\%$ for Be, $< 0.6\%$ for Li, B, and N, and negligible for C and O over the entire rigidity range.

For all nuclei, the rigidity resolution function has a pronounced Gaussian core characterized by width σ and non-Gaussian tails more than 2.5σ away from the center [7–9]. The systematic error on the fluxes due to the rigidity resolution function was obtained by repeating the unfolding procedure while varying the width of the Gaussian core of the resolution function by 5% and by independently varying the amplitude of the non-Gaussian tails by 10% [7–9]. The resulting time-independent systematic error in the flux is $< 1\%$ over the entire rigidity range for all nuclei. The flux variation per Bartels rotation leads to an additional uncertainty in the unfolding procedure. The resulting

time-dependent systematic error is $< 1\%$ for all nuclei at 1.92 GV and negligible above 5 GV for all Bartels rotations.

The systematic error of the unfolding procedure due to uncertainties in the acceptance in the lowest rigidity bin was found to be negligible for He, $< 2\%$ for Li, Be, B, $< 1.5\%$ for C, $< 5\%$ for N and O, and negligible for all nuclei above 2.4 GV.

There are two contributions to the systematic uncertainty on the rigidity scale [6]: the first is due to residual tracker misalignment and the second to the magnetic field map measurement and its temperature corrections. Both effects give a negligible systematic error on all fluxes over the entire rigidity range.

The overall time-independent systematic error is obtained by adding in quadrature the individual independent contributions of the background subtraction, due to uncertainties in the evaluation of the inelastic cross sections and trigger, reconstruction, and selection efficiencies.

The overall time-dependent systematic error is obtained, for each Bartels rotation, by adding in quadrature the individual independent contributions of unfolding and the time dependence of the reconstruction and selection efficiencies.

Most important, several independent analyses were performed on the same data sample by different study groups. The results of those analyses are consistent with this Letter.

Results—The measured He flux including statistical and systematic errors is tabulated in Tables S1–S147 in the SM [18,28] for Bartels rotations 2426 to 2581, as a function of the rigidity at the top of the AMS detector. Previously, AMS has made extensive studies of the time variation of the He flux [14]. The current measurements cover an extended time range and are in agreement with our previous measurements in the overlapping time period. The measured Li, Be, B, C, N, and O fluxes including statistical and systematic errors are tabulated in Tables S148–S1029 in the SM [18,28] for Bartels rotations 2426 to 2581, as a function of the rigidity at the top of the AMS detector. To compare with the He flux variations we also tabulate the Li/He, Be/He, B/He, C/He, N/He, and O/He flux ratios as a function of rigidity in Tables S148–S1029 in the SM [18,28].

Figure 1 shows the AMS Li, Be, B, C, N, and O fluxes as a function of time for the lowest rigidity interval from 1.92 to 2.15 GV together with the He flux. As seen, the nuclei fluxes exhibit similar short- and long-term temporal structures with respect to the He flux.

Figures S3 to S8 of the SM [18] show the six nuclei fluxes as a function of time for four characteristic rigidity bins up to 60.3 GV. As seen, the amplitude of the time structures decreases with increasing rigidity.

To determine the rigidity range in which the time variations of the nuclei fluxes are observable, in each of the 40 rigidity bins we fitted the time variation of 147 Bartels rotations with the average value of the 147 Bartels rotations and we tested the χ^2. We found that at a 3σ level the time structures can be observed up to 48.5 GV for He, 14.1 GV for Li, 13.0 GV for Be, 15.3 GV for B, 21.1 GV for C, 16.6 GV for N, and 24.7 GV for O.

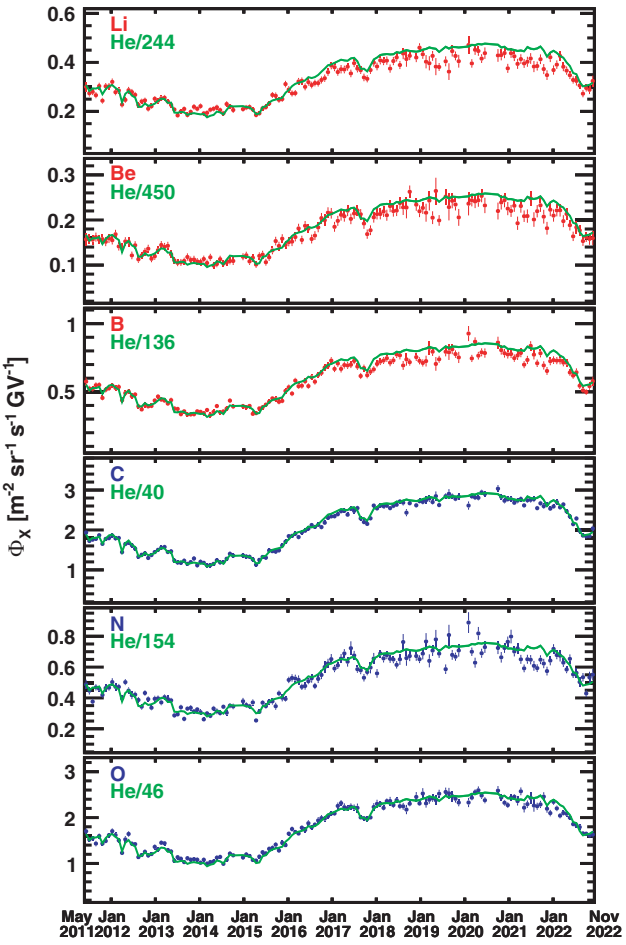

FIG. 1. The He, Li, Be, B, C, N, and O fluxes measured by AMS with rigidities between 1.92 and 2.15 GV in 147 Bartels rotations from May 2011 to Nov 2022 as a function of time. The He flux (green curves) has been scaled in each panel to the average of the displayed flux. As seen, all fluxes show similar but not identical time behavior.

Figure 2 shows the ratio of each nuclei flux to the He flux as a function of rigidity. The bands show the time variation range of the flux ratios due to solar modulation. To compare in detail the time variation of nuclei fluxes with that of the He flux, we fit a linear relation between the relative variation of the flux ratio of the nucleus X and the He flux $\Phi_X/\Phi_{\mathrm{He}}$, as a function of the relative variation of the He flux Φ_{He} for each ith rigidity bin,

$$\frac{\Phi^i_X/\Phi^i_{\mathrm{He}} - \langle \Phi^i_X/\Phi^i_{\mathrm{He}} \rangle}{\langle \Phi^i_X/\Phi^i_{\mathrm{He}} \rangle} = K^i_{X/\mathrm{He}} \frac{\Phi^i_{\mathrm{He}} - \langle \Phi^i_{\mathrm{He}} \rangle}{\langle \Phi^i_{\mathrm{He}} \rangle}, \quad (2)$$

where $K^i_{X/\mathrm{He}}$ is the slope of the $\Phi_X/\Phi_{\mathrm{He}}$ linear dependence, and $\langle \Phi^i_X/\Phi^i_{\mathrm{He}} \rangle$ and $\langle \Phi^i_{\mathrm{He}} \rangle$ are respectively the averaged flux

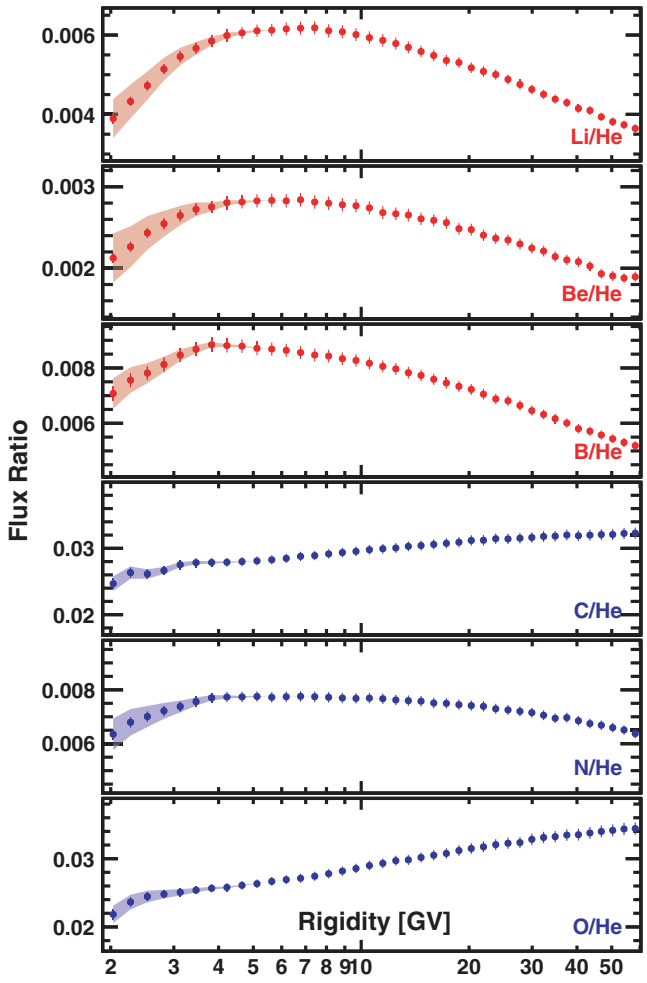

FIG. 2. The AMS time-averaged Li/He, Be/He, B/He, C/He, N/He, and O/He flux ratios in the rigidity range from 1.92 to 60.3 GV. The shaded bands show the observed time variation range.

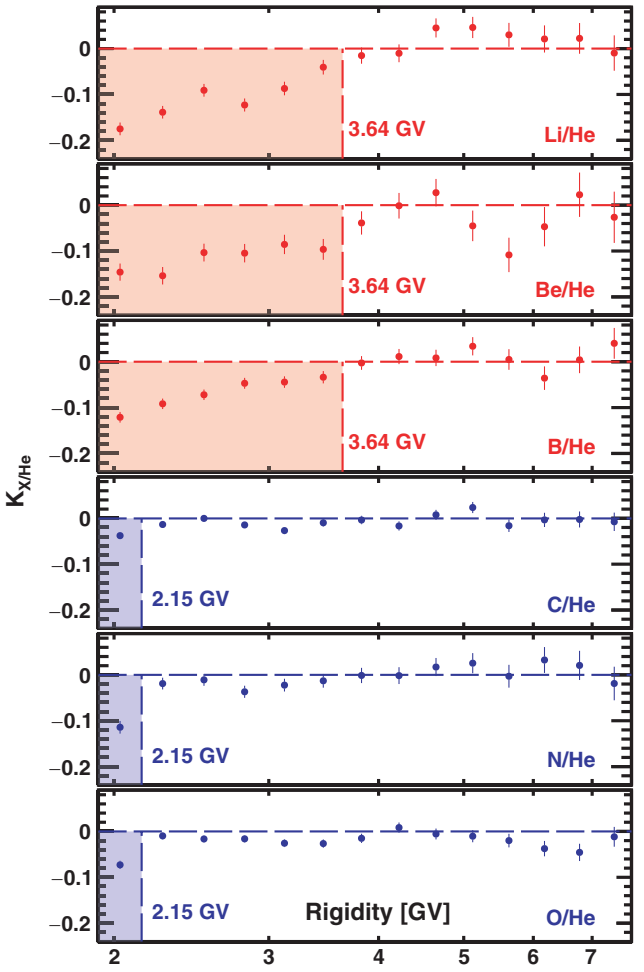

FIG. 3. The relative solar modulation magnitude $K_{X/He}$ as a function of rigidity derived from fits to Eq. (2). As seen up to 3.64 GV, Li, Be, and B are significantly less modulated than He ($K_{X/He} < 0$), and, up to 2.15 GV, C, N, and O are significantly less modulated than He.

ratio and the averaged He flux over the entire period of 11.5 yr, similar to Ref. [16]. $K^i_{X/He} \neq 0$ signifies a difference in solar modulation between the nucleus X and He fluxes. Figure 3 shows the measured $K^i_{X/He}$ as a function of rigidity. As seen, $K_{Li/He}$, $K_{Be/He}$, and $K_{B/He}$ are significantly below zero for rigidities from 1.92 to 3.64 GV showing that Li, Be, and B fluxes are less modulated than the He flux. The relatively large variations of $K_{Be/He}$ above 3.64 GV with respect to other $K_{X/He}$ (see panel 2 of Fig. 3) are due to the much lower statistics of Be nuclei. $K_{C/He}$, $K_{N/He}$, and $K_{O/He}$ are significantly below zero in the rigidity bin from 1.92 to 2.15 GV showing that C, N, and O fluxes are also less modulated than the He flux in this rigidity range.

To determine the difference in the solar modulation of nuclei flux due to differences in their spectral shape, in a model-independent way, the spectral indices $\Delta_{X/He}$ of the flux ratios have been calculated as a function of rigidity using

$$\Delta_{X/He} = \frac{d \log\langle \Phi_X/\Phi_{He}\rangle}{d \log R}, \quad (3)$$

in consecutive ranges of three rigidity bins. Figure S9 of the SM [18] shows the spectral index as a function of rigidity. As seen, below 3.64 GV, the spectral indices of Li/He, Be/He, and B/He flux ratios and, below 2.15 GV, the spectral indices of C/He, N/He, and O/He flux ratios are greater than zero, showing that He flux rigidity dependence is steeper (i.e., decreasing more quickly) than that of Li, Be, B, C, N, and O fluxes in these rigidity ranges.

The obtained relative solar modulation magnitude $K_{X/He}$ as a function of $\Delta_{X/He}$ has been studied as a function of rigidity (see Fig. S10 of SM [18]), and a significant correlation is observed between the two variables up to 3.64 GV. To obtain the relation between the two variables we fit a linear dependence $K_{X/He} = \xi \Delta_{X/He}$. Table I shows the values of ξ for the six lowest rigidity bins. Remarkably,

TABLE I. Results of the fits $K_{X/\mathrm{He}} = \xi\Delta_{X/\mathrm{He}}$ to the data in the six lowest rigidity bins. This shows that ξ is consistent with a rigidity-independent average value of -0.175 ± 0.010.

R (GV)	ξ
1.92–2.15	-0.18 ± 0.02
2.15–2.40	-0.18 ± 0.02
2.40–2.67	-0.14 ± 0.02
2.67–2.97	-0.20 ± 0.02
2.97–3.29	-0.19 ± 0.03
3.29–3.64	-0.17 ± 0.04

all ξ are consistent with a rigidity-independent average value of -0.175 ± 0.010. A negative ξ means fluxes are more modulated for nuclei with steeper spectra.

Because of the different isotopic composition, for the same rigidity, Li, Be, B, C, N, and O have lower average velocities than He, traveling for more time in the heliosphere and therefore should exhibit more modulation than He due to the velocity effect.

To estimate the magnitude of the velocity effect in a model-independent way, we compared the time variations of Be, C, and O fluxes with that of the ^{4}He flux from Ref. [15] in the lowest rigidity bin 1.92 to 2.15 GV, with 10 yr of data and with four Bartels rotation time window using Eq. (2), where He was replaced with ^{4}He. As all four nuclei have the same velocity for the same rigidity [29], the solar modulation velocity effect is negligible. As seen in Fig. 4 the obtained $K_{\mathrm{Be}/^4\mathrm{He}}$, $K_{\mathrm{C}/^4\mathrm{He}}$, and $K_{\mathrm{O}/^4\mathrm{He}}$ are compatible respectively with $K_{\mathrm{Be/He}}$, $K_{\mathrm{C/He}}$, and $K_{\mathrm{O/He}}$, showing that the velocity effect is small. Most importantly, fitting the linear relation $K_{X/^4\mathrm{He}} = \xi'\Delta_{X/^4\mathrm{He}}$ we obtained $\xi' = -0.16 \pm 0.04$, again compatible with the corresponding ξ value of -0.18 ± 0.02 (see Table I in the first rigidity bin).

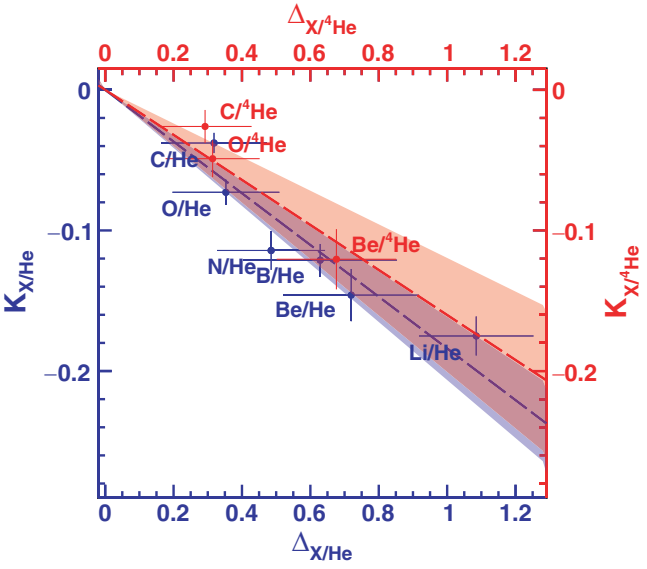

FIG. 4. The dependence of the relative solar modulation magnitude $K_{X/\mathrm{He}}$ on the spectral index $\Delta_{X/\mathrm{He}}$ for the rigidity bin 1.92 to 2.15 GV for Li/He, Be/He, B/He, C/He, N/He, and O/He flux ratios (in blue). A linear fit with the function $K_{X/\mathrm{He}} = \xi\Delta_{X/\mathrm{He}}$ with $\xi = -0.18 \pm 0.02$ (χ^2/d.o.f. $= 1.8/5$) is also shown as a blue dashed line and 1σ shade. The dependence of the relative solar modulation magnitude $K_{X/^4\mathrm{He}}$ on the spectral index $\Delta_{X/^4\mathrm{He}}$ for the rigidity bin 1.92 to 2.15 GV for Be/^{4}He, C/^{4}He, and O/^{4}He flux ratios (in red), for which the solar modulation velocity effect is negligible. A linear fit with the function $K_{X/^4\mathrm{He}} = \xi'\Delta_{X/^4\mathrm{He}}$ with $\xi' = -0.16 \pm 0.04$ (χ^2/d.o.f. $= 0.8/2$) is also shown as a red dashed line and 1σ shade. As seen, the ξ and ξ' are compatible.

In conclusion, the He, Li, Be, B, C, N, and O fluxes and the Li/He, Be/He, B/He, C/He, N/He, and O/He flux ratios have been precisely measured in 147 Bartels rotations from May 2011 to November 2022 in the rigidity range from 1.92 to 60.3 GV with the Alpha Magnetic Spectrometer. The nuclei fluxes show similar but not identical time variations with amplitudes decreasing with increasing rigidity. In particular, below 3.64 GV, the Li, Be, and B fluxes, and, below 2.15 GV, the C, N, and O fluxes, are significantly less affected by solar modulation than the He flux. We observe that these differences in solar modulation are linearly correlated with the differences in the spectral indices of the nuclei fluxes. This shows, in a model-independent way, that solar modulation of galactic cosmic nuclei depends on their spectral shape. In addition, solar modulation differences due to nuclei velocity dependence on the mass-to-charge ratio (A/Z) are not observed.

Acknowledgments—We are grateful for important physics discussions with Igor Moskalenko. We thank former NASA Administrator Daniel S. Goldin for his dedication to the legacy of the ISS as a scientific laboratory and his decision for NASA to fly AMS as a DOE payload. We also acknowledge the continuous support of the NASA leadership, particularly Ken Bowersox and of the JSC and MSFC flight control teams that have allowed AMS to operate optimally on the ISS for over 13 years. We are grateful for the support of Regina Rameika and Glen Crawford of the DOE including resources from the National Energy Research Scientific Computing Center under Contract No. DE-AC02-05CH11231. We gratefully acknowledge the strong support from CERN, including Fabiola Gianotti, and the CERN IT department, including Bernd Panzer-Steindel. We also acknowledge the continuous support from MIT and its School of Science, Nergis Mavalvala, and the Laboratory for Nuclear Science, Boleslaw Wyslouch. Research supported by Chinese Academy of Sciences, Institute of High Energy Physics, National Natural Science Foundation (NSFC), and Ministry of Science and Technology, National Key R&D Program Grants No. 2022YFA1604802 and No. 2022YFA1604803, NSFC Grant No. 12275158, the China Scholarship Council, the provincial governments of Shandong,

Jiangsu, Guangdong, Shandong University, and the Shandong Institute of Advanced Technology, China; Research Council of Finland, Project No. 321882, and Finnish Academy of Sciences and Letters, Grant No. 301123, Finland; CNRS/IN2P3 and CNES, France; DLR under Grant No. 50OO1803 and computing support on the JARA Partition of the RWTH Aachen supercomputer, Germany; INFN and ASI under ASI-INFN Agreements No. 2019-19-HH.0, its amendments, No. 2021-43-HH.0, and ASI-University of Perugia Agreement No. 2019-2-HH.0, and the Italian Ministry of University and Research (MUR) through the program *"Dipartimenti di Eccellenza 2023-2027"* (Grant SUPER-C), Italy; the Consejo Nacional de Humanidades, Ciencias y Tecnologías (CONAHCYT) under Grant No. CF-2019/2042 and UNAM, Mexico; NWO under Grant No. 680-1-004, Netherlands; FCT under Grant No. CERN/FIS-PAR/0013/2019, Portugal; CIEMAT, IAC, CDTI, MCIN-AEI, and ERDF under Grants No. PID2022-137810NB-C21/C22, No. PCI2023-145945-2, No. PCI2023-145961-2, No. CEX2019-000920-S, and No. JDC2022-049705-I, Spain; the Fondation Dr. Manfred Steuer and the Fondation Ernst et Lucie Schmidheiny, Switzerland; Academia Sinica, the National Science and Technology Council (NSTC), formerly the Ministry of Science and Technology (MOST), under Grants No. 111-2123-M-001-004 and No. 111-2112-M-006-029, High Education Sprout Project by the Ministry of Education at National Cheng Kung University, former Presidents of Academia Sinica Yuan-Tseh Lee and Chi-Huey Wong and former Ministers of NSTC (formerly MOST) Maw-Kuen Wu and Luo-Chuan Lee, Taiwan; the Turkish Energy, Nuclear and Mineral Research Agency (TENMAK) under Grant No. 2020TAEK(CERN)A5.H1.F5-26, Türkiye; and NSF Grant No. 2013228 and ANSWERS proposals No. 2149809, No. 2149810, and No. 2149811, LWS NASA Grant/Cooperative Agreement No. 80NSSC20K1819, and FINESST NASA Grant No. 80NSSC21K1392, USA.

[1] E. N. Parker, The passage of energetic charged particles through interplanetary space, Planet. Space Sci. **13**, 9 (1965).
[2] M. S. Potgieter, Solar modulation of cosmic rays, Living Rev. Solar Phys. **10**, 3 (2013).
[3] C. Corti, M. S. Potgieter, V. Bindi, C. Consolandi, C. Light, M. Palermo, and A. Popkow, Numerical modeling of galactic cosmic-ray proton and helium observed by AMS-02 during the solar maximum of solar cycle 24, Astrophys. J. **871**, 253 (2019).
[4] N. Tomassetti, F. Barão, B. Bertucci, E. Fiandrini, and M. Orcinha, Numerical modeling of cosmic-ray transport in the heliosphere and interpretation of the proton-to-helium ratio in Solar Cycle 24, Adv. Space Res. **64**, 2477 (2019).
[5] M. D. Ngobeni, O. P. M. Aslam, D. Bisschoff, M. S. Potgieter, D. C. Ndiitwani, M. Boezio, N. Marcelli, R. Munini, V. V. Mikhailov, and S. A. Koldobskiy, The 3D numerical modeling of the solar modulation of galactic protons and helium nuclei related to observations by PAMELA between 2006 and 2009, Astrophys. Space Sci. **365**, 182 (2020).
[6] M. Aguilar *et al.*, The Alpha Magnetic Spectrometer (AMS) on the International Space Station: Part II—results from the first seven years, Phys. Rep. **894**, 1 (2021).
[7] M. Aguilar *et al.*, Observation of the identical rigidity dependence of He, C, and O cosmic rays at high rigidities by the Alpha Magnetic Spectrometer on the International Space Station, Phys. Rev. Lett. **119**, 251101 (2017).
[8] M. Aguilar *et al.*, Observation of new properties of secondary cosmic rays Lithium, Beryllium, and Boron by the Alpha Magnetic Spectrometer on the International Space Station, Phys. Rev. Lett. **120**, 021102 (2018).
[9] M. Aguilar *et al.*, Precision measurement of cosmic-ray nitrogen and its primary and secondary components with the Alpha Magnetic Spectrometer on the International Space Station, Phys. Rev. Lett. **121**, 051103 (2018).
[10] M. Aguilar *et al.*, Temporal structures in positron spectra and charge-sign effects in galactic cosmic rays, Phys. Rev. Lett. **131**, 151002 (2023).
[11] M. Aguilar *et al.*, Temporal structures in electron spectra and charge sign effects in galactic cosmic rays, Phys. Rev. Lett. **130**, 161001 (2023).
[12] M. Aguilar *et al.*, Periodicities in the daily proton fluxes from 2011 to 2019 measured by the Alpha Magnetic spectrometer on the International Space Station from 1 to 100 GV, Phys. Rev. Lett. **127**, 271102 (2021).
[13] M. Aguilar *et al.*, Antiprotons and elementary particles over a solar cycle: Results from the Alpha Magnetic Spectrometer (to be published) [Phys. Rev. Lett.].
[14] M. Aguilar *et al.*, Properties of daily helium fluxes, Phys. Rev. Lett. **128**, 231102 (2022).
[15] M. Aguilar *et al.*, Properties of cosmic helium isotopes measured by the Alpha Magnetic Spectrometer, Phys. Rev. Lett. **123**, 181102 (2019).
[16] M. Aguilar *et al.*, Properties of cosmic deuterons measured by the Alpha Magnetic Spectrometer, Phys. Rev. Lett. **132**, 261001 (2024).
[17] A. Kounine, The Alpha Magnetic Spectrometer on the International Space Station, Int. J. Mod. Phys. E **21**, 1230005 (2012).
[18] See Supplemental Material at http://link.aps.org/supplemental/10.1103/PhysRevLett.134.051001 for additional details and figures on the detector, event selection, and results, and, for Bartels rotations from 2426 to 2581, the tabulated He flux, and the tabulated Li, Be, B, C, N, O fluxes and their flux ratios to He. Data for Bartels rotations 2472, 2473, 2526, 2535, 2541, 2542, 2549, 2550, and 2551 are not provided as AMS was not operating in nominal conditions.
[19] K. Lübelsmeyer *et al.*, Upgrade of the Alpha Magnetic Spectrometer (AMS-02) for long term operation on the International Space Station (ISS), Nucl. Instrum. Methods Phys. Res., Sect. A **654**, 639 (2011).
[20] B. Alpat *et al.*, The internal alignment and position resolution of the AMS-02 silicon tracker determined with cosmic-ray muons, Nucl. Instrum. Methods Phys. Res., Sect. A **613**, 207 (2010).
[21] V. Bindi *et al.*, Calibration and performance of the AMS-02 time of flight detector in space, Nucl. Instrum. Methods Phys. Res., Sect. A **743**, 22 (2014).

[22] J. Allison *et al.*, Recent developments in GEANT4, Nucl. Instrum. Methods Phys. Res., Sect. A **835**, 186 (2016); GEANT4 developments and applications, IEEE Trans. Nucl. Sci. **53**, 270 (2006); S. Agostinelli *et al.*, GEANT4—a simulation toolkit, Nucl. Instrum. Methods Phys. Res., Sect. A **506**, 250 (2003).

[23] M. Aguilar *et al.*, Precision measurement of the helium flux in primary cosmic rays of rigidities 1.9 GV to 3 TV with the Alpha Magnetic Spectrometer on the International Space Station, Phys. Rev. Lett. **115**, 211101 (2015).

[24] Y. Jia, Q. Yan, V. Choutko, H. Liu, and A. Oliva, Nuclei charge measurement by the Alpha Magnetic Spectrometer silicon tracker, Nucl. Instrum. Methods Phys. Res., Sect. A **972**, 164169 (2020).

[25] G. Ambrosi, V. Choutko, C. Delgado, A. Oliva, Q. Yan, and Y. Li, The spatial resolution of the silicon tracker of the Alpha Magnetic Spectrometer, Nucl. Instrum. Methods Phys. Res., Sect. A **869**, 29 (2017).

[26] P. Alken *et al.*, International geomagnetic reference field: The thirteenth generation, Earth Planets Space **73**, 49 (2021).

[27] Q. Yan, V. Choutko, A. Oliva, and M. Paniccia, Measurements of nuclear interaction cross sections with the Alpha Magnetic Spectrometer on the International Space Station, Nucl. Phys. **A996**, 121712 (2020).

[28] Note that the data can also be downloaded in different formats from the AMS website https://ams02.space/sites/default/files/publication/202403/table-S1-S147.csv, table-S148-S294.csv, table-S295-S441.csv, table-S442-S588.csv, table-S589-S735.csv, table-S736-S882.csv, table-S883-S1029.csv, the ASI cosmic-ray database at https://tools.ssdc.asi.it/CosmicRays, and the LPSC cosmic-ray database at https://lpsc.in2p3.fr/crdb/.

[29] M. Aguilar *et al.*, Properties of light nuclei isotopes measured by the Alpha Magnetic Spectrometer (to be published).